TITLE PAGE

A Pan-Cyclophilin Inhibitor, CRV431, Decreases Fibrosis and Tumor Development in Chronic Liver Disease Models

Joseph Kuo, Michael Bobardt, Udayan Chatterji, Patrick R. Mayo, Daniel J. Trepanier, Robert T. Foster, Philippe Gallay, Daren R. Ure

Department of Immunology & Microbiology, The Scripps Research Institute, La Jolla, California 92037, USA (J.K., M.B., U.C., P.G.)

ContraVir Pharmaceuticals Inc., Edison, New Jersey 08837, USA (P.M., D.J.T., R.T.F., D.R.U.)

Primary laboratory of origin: Contravir Pharmaceuticals, Edmonton, Alberta, Canada

RUNNING TITLE PAGE

Running title: CRV431 decreases liver fibrosis and tumor development

Corresponding author*:*

Daren Ure, Contravir Pharmaceuticals, 2011 – 94th Street NW, Edmonton, Alberta, Canada T6N 1H1

dure@contravir.com ; Ph 587-754-9554; FAX 587-754-7533

Second corresponding author on published manuscript:

Philippe Gallay, Department of Immunology & Microbiology, The Scripps Research Institute, 10550 North Torrey Pines Road, La Jolla, California 92037, USA

gallay@scripps.edu; Ph (858) 784 8180; FAX (858) 784 8115

Number of text pages: 36

Number of tables: 5

Number of figures: 6

Number of references: 66

Number of words in Abstract: 237

Number of words in Introduction: 724

Number of words in Discussion: 1499

Recommended section: Gastrointestinal, Hepatic, Pulmonary, and Renal

JPET Fast Forward. Published on August 12, 2019 as DOI: 10.1124/jpet.119.261099
This article has not been copyedited and formatted. The final version may differ from this version.

Abbreviations:

ABC	ATP-binding cassette transporter
ABCB1	ATP-binding cassette sub-family B member 1
AP-1	Activating protein-1
BCRP	breast cancer resistance protein, gene symbol ABCG2
BSA	bovine serum albumin
BSEP	bile salt export pump, gene symbol ABCB11
CCl_4	carbon tetrachloride
CL/F	drug clearance after oral administration
DMSO	dimethyl sulfoxide
FBS	fetal bovine serum
HEK293	human embryonic kidney cells
HEPES	N-[2-Hydroxyethyl]piperazine-N'-[2-ethanesulfonic acid]
HFD	high fat diet
HPLC	high performance liquid chromatography
IC50	concentration at 50% inhibition
IL-2	interleukin-2
Km	Michaelis constant; substrate concentration at half-maximal reaction rate
MATE1	multidrug and toxin extrusion protein 1, gene symbol SLC47A1
MATE2-K	multidrug and toxin extrusion protein 2-K, gene symbol SLC47A2
MDCKII	Madin-Darby Canine Kidney cells
MMP	matrix metalloproteinase
MRP2	multidrug resistance protein 2
n	number of replicates
n/a	not applicable

NFAT	nuclear factor of activated T-cells
NF-κB	nuclear factor kappa-light-chain-enhancer of activated B cells
NTCP1	sodium-dependent taurocholic acid co-transporting polypeptide 1
OAT1	organic anion transporter 1, gene symbol SLC22A6
OAT3	organic anion transporter 3, gene symbol SLC22A8
OATP1B1	organic anion transporting polypeptide 1B1, gene symbol SLCO1B1
OATP1B3	organic anion transporting polypeptide 1B3, gene symbol SLCO1B3
OCT2	organic cation transporter 2, gene symbol SLC22A2
PBS	phosphate buffered saline
P-gp	permeability-glycoprotein, (multidrug resistance protein 1)
PMA	phorbol myristate acetate
TIMP-1	tissue inhibitor of metalloproteinase-1
Vmax	maximum velocity

JPET Fast Forward. Published on August 12, 2019 as DOI: 10.1124/jpet.119.261099
This article has not been copyedited and formatted. The final version may differ from this version.

ABSTRACT

Previous studies show that cyclophilins contribute to many pathological processes, and cyclophilin inhibitors demonstrate therapeutic activities in many experimental models. However, no drug with cyclophilin inhibition as the primary mode of action has advanced completely through clinical development to market. Here we present findings on the cyclophilin inhibitor, CRV431, that highlight its potential as a drug candidate for chronic liver diseases. CRV431 was found to potently inhibit all cyclophilin isoforms tested - A, B, D, and G. Inhibitory constant or IC_{50} values ranged from 1-7 nM which was up to 13 times more potent than the parent compound, cyclosporine A (CsA), from which CRV431 was derived. Other CRV431 advantages over CsA as a non-transplant drug candidate were significantly diminished immunosuppressive activity, less drug transporter inhibition, and reduced cytotoxicity potential. Oral dosing to mice and rats led to good blood exposures and a 5-15-fold accumulation of CRV431 in liver compared to blood concentrations across a wide range of CRV431 dosing levels. Most importantly, CRV431 decreased liver fibrosis in a 6-week carbon tetrachloride model and in a mouse model of non-alcoholic steatohepatitis (NASH). Additionally, CRV431 administration during a late, oncogenic stage of the NASH disease model resulted in a 50% reduction in the number and size of liver tumors. These findings are consistent with CRV431 targeting fibrosis and cancer through multiple, cyclophilin-mediated mechanisms and support the development of CRV431 as a safe and effective drug candidate for liver diseases.

JPET Fast Forward. Published on August 12, 2019 as DOI: 10.1124/jpet.119.261099
This article has not been copyedited and formatted. The final version may differ from this version.

SIGNIFICANCE

Cyclophilin inhibitors have demonstrated therapeutic activities in many disease models, but no drug candidates have yet advanced completely through development to market. Here CRV431 is shown to potently inhibit multiple cyclophilin isoforms, possess several optimized pharmacological properties, and decrease liver fibrosis and tumors in mouse models of chronic liver disease, which highlights its potential to be the first approved drug primarily targeting cyclophilin isomerases.

INTRODUCTION

Cyclophilin A (Cyp A) was first isolated in 1984 and fittingly named for its feature characteristic - binding to the potent immunosuppressant, cyclosporin A (CsA). Cyclophilin A is also known as peptidyl prolyl isomerase A (PPIA) because its primary biochemical activity is catalytic regulation of *cis-trans* isomerization of X-proline peptide bonds (where X represents any amino acid) which are important for protein folding and function. Eighteen human proteins with cyclophilin isomerase domains exist and occupy many cellular compartments (Davis *et al.*, 2010; Lavin and McGee, 2015). The best described isoforms include cyclophilin A (PPIA; cytosol), cyclophilin B (PPIB; endoplasmic reticulum), and cyclophilin D (PPIF; mitochondria). Cyclophilins have important roles in normal physiological function but they also participate in many pathological processes (Nigro *et al.*, 2013; Naoumov, 2014; Xue *et al.*, 2018; Briston *et al.*, 2019). For example, cyclophilin D (Cyp D) is a primary inducer of mitochondrial permeability transition which leads to cell death after a variety of cellular insults. Cyclophilin A (Cyp A) has been evolutionarily recruited into the life cycles of many viruses such as hepatitis B and C viruses (Ullah Dawar *et al.*, 2017). Overexpression of cyclophilins has been observed in many types of cancer, which appears to facilitate adaptation to hypoxia and elevated anabolic demands (Lavin and McGee, 2015). Extracellular Cyp A released from injured or dying cells can be pro-inflammatory through its binding to CD147. Cyclophilin B (Cyp B), while important for collagen production and maturation throughout development, may exacerbate fibrotic pathologies characterized by excessive collagen production. Thus, pharmacological inhibitors of cyclophilins have the potential to be broadly therapeutic across a spectrum of diseases and disorders.

Two major pathologies to which cyclophilins are believed to contribute are fibrosis and cancer. In the liver, fibrosis commonly develops in all the major forms of chronic hepatitis – alcoholic,

non-alcoholic, and viral – and is a primary predictor of cirrhosis, hepatocellular carcinoma (HCC), and mortality. Excessive deposition of extracellular matrix can profoundly change the anatomy and physiology of the liver and create an environment that promotes malignancy. HCC is the most common type of primary liver cancer, has a poor prognosis, and annually accounts for approximately 800,000 deaths worldwide (Kulik and El-Serag, 2019). New treatments that positively shift the fibrogenesis-fibrolysis dynamic towards decreasing fibrosis and lowering the risk of HCC are urgently needed.

The most thoroughly characterized chemical class of cyclophilin inhibitors are the cyclosporins. The prototypical inhibitor, cyclosporin A (CsA), is an 11-amino acid cyclic peptide which revolutionized solid organ transplantation after its approval as an immunosuppressant in 1983. The mechanism of immunosuppression is binding of CsA to cyclophilin A, followed by CsA-Cyp A dimer binding to, and inhibition of the lymphocyte-activating phosphatase, calcineurin. Whereas CsA is a potent inhibitor of cyclophilins, its immunosuppressive activity largely limits its therapeutic use as a cyclophilin inhibitor. To address this limitation, many compounds have been produced that antagonize cyclophilins but without significant calcineurin inhibition (Sweeney *et al.*, 2014; Dunyak and Gestwicki, 2016). Nonimmunosuppressive analogs of CsA comprise the largest class, and notable representatives are valspodar, NIM811, EDP-546, SCY635, MM284, and alisporivir (DEBIO-025). Alisporivir demonstrated the most clinical potential by advancing through Phase 2 clinical trials with robust antiviral activity toward hepatitis C virus (Buti *et al.*, 2015; Pawlotsky *et al.*, 2015). Cyclophilin inhibitors also have been derived from other chemical platforms – small molecules or derivatives of the macrolide, sanglifehrin A – but they often have shown lower potency than cyclosporin compounds, poor bioavailability, or have not been extensively characterized (Moss *et al.*, 2012; Sweeney *et al.*, 2014; Yan *et al.*, 2015). Despite this diversity of cyclophilin inhibitors, none have advanced completely through clinical development to market.

CRV431 is a CsA analog that is unique from most previously described derivatives, as a result of chemical substitutions made at amino acids 1 and 3 of the cyclosporine ring (Trepanier *et al.*, 2018). Its antiviral activities towards HBV, HCV and HIV-1 and other properties have previously been reported (Gallay *et al.*, 2015, 2019). The present report further documents activities of CRV431 that distinguish it from other members of the cyclosporin class. The data reinforce the potential of pan-cyclophilin inhibitors as safe, therapeutic agents. We show that CRV431 decreases liver fibrosis in two animal models and decreases liver tumor burden in a mouse model of non-alcoholic steatohepatitis (NASH), which highlights its potential as a treatment for liver disease of various etiologies.

JPET Fast Forward. Published on August 12, 2019 as DOI: 10.1124/jpet.119.261099
This article has not been copyedited and formatted. The final version may differ from this version.

MATERIALS AND METHODS

CRV431 and CsA Solutions

For all *in vitro* experiments CRV431 and CsA stock solutions in DMSO (Sigma, D2650) were prepared first at concentrations up to 80 mM, followed by at least 500-fold dilution into buffers or cell culture medium to create the working solutions. DMSO was used as the vehicle control in all *in vitro* experiments at the same dilutions as were used in making the CRV431 working solutions. The maximum working solution concentration of CRV431 in aqueous medium was 80 µM (cytotoxicity assays), which was determined by HPLC analysis to be below the limit of aqueous solubility (115 µM) and completely soluble (Trepanier *et al.*, 2018). The maximum attempted working solution concentration of CsA in aqueous medium was 80 µM (cytotoxicity assays), but HPLC analysis determined a maximum CsA solubility of 31.9 µM (Trepanier *et al.*, 2018).

Cyclophilin Isomerase Assay

Cyclophilin isomerase activity was measured with an assay described by Kofron et al. (1991) with adaptations to 96-well plates. In this assay cyclophilins catalyze *cis*-to-*trans* isomerization of a proline peptide bond in a nitroanalide-coupled peptide substrate followed by cleavage of the *trans*-conformer peptide by α-chymotrypsin, release of the *p*-nitroaniline chromogen, and quantitation of *p*-nitroaniline by absorbance at 410 nm. All solutions were pre-equilibrated and all assays conducted at 4˚C. Plates were pre-loaded with 5 µl peptide solution consisting of N-succinyl-alanine-alanine-proline-phenylalanine-*p*-nitroanilide (Sigma, S7388) and 400 mM lithium chloride (Sigma, 310468) in anhydrous trifluoroethanol (Sigma, T63002). Eight peptide concentrations spanning 100-1000 µM were tested for inhibitory constant (Ki) determinations, and a single peptide concentration, 150 µM, was used for IC_{50} determinations. *Cis*-peptide represented 55% of the peptide isomers, based on initial reaction bursts, and therefore peptide

concentration was corrected to 55% of input in subsequent calculations. Reactions were initiated by thoroughly mixing in 95 µl of reaction mix consisting of 50 mM Hepes (pH 8.0), 100 mM NaCl, 20 nM recombinant cyclophilin A (R&D Systems 3589-CAB), cyclophilin B (Cedarlane Labs, CLENZ313), cyclophilin D (Cedarlane Labs, CLENZ385), or cyclophilin G (Cedarlane Labs, CLENZ463), 1 mg/mL α-chymotrypsin (Sigma C4129), 5 mg/ml human serum albumin (Sigma, A1653), and 3-fold serial dilutions of CRV431 and CsA spanning 0.05 – 1000 nM. Absorbance measurements with a BMG Polarstar Galaxy plate reader were begun immediately and made at 6 second intervals for 6 minutes. Reaction curves were represented by increases in OD410 nm as a function of reaction time. For Ki determinations, initial reaction velocities were obtained from the reaction curves, plotted relative to substrate concentration, and the curves fitted to the enzyme competitive inhibition model (Graphpad Prism) to derive Ki, Vmax, and Km values. For IC_{50} determinations the reaction curves were fitted to one-phase exponential association regressions to obtain first-order rate constants. Catalytic rate constants were calculated by subtracting the uncatalyzed reaction rate constants (no cyclophilin plotted as a function of CRV431 or CsA concentration and fitted by sigmoidal dose-response regressions to obtain IC_{50} values.

NFAT and IL-2 Luciferase Reporter Assays

The luciferase reporter assays employed Jurkat cells stably transfected with gene constructs consisting of a luciferase gene plus human NFAT or IL-2 promoter elements (Promega, J1621 and J1651). The NFAT construct contained a DNA binding site only for NFAT, whereas the IL-2 construct contained binding sites for NFAT, NF-kB and AP-1 transcription factors. Cells were cultured in 96-well plates at 100,000 cells per well in RPMI 1640 medium (Thermo Fisher, 11875-093) supplemented with 5% FBS (Thermo Fisher, 12483020). Cells were activated either by pre-coating high protein binding plates with 3 µg/ml anti-CD3 (UCHT clone) and anti-CD28 (CD28.2 clone) (BioLegend LEAF antibodies) or by adding phorbol myristate acetate (PMA;

JPET Fast Forward. Published on August 12, 2019 as DOI: 10.1124/jpet.119.261099
This article has not been copyedited and formatted. The final version may differ from this version.

Sigma, P8139) to 15 ng/ml and A23187 ionophore (Sigma C7522) to 0.75 µM. DMSO, CRV431, or CsA were included across a range of concentrations. Cells were harvested after 18 hr of incubation, and luciferase quantified with Promega Bio-Glo reagent (Promega G7940) and measurement with a luminescence plate reader. Data were normalized to DMSO controls (100% stimulation) and to wells without antibody or PMA+A23187 stimulation.

CFSE-PBMC Proliferation

Peripheral blood mononuclear cells (PBMC) were isolated by Ficoll Paque Plus centrifugation (GE Life Sciences, 17144003) of venous blood from a healthy human male volunteer. Cells were incubated for 5 minutes with 5 µg/mL carboxyfluorescein diacetate succinimidyl ester (CFDA-SE; Thermo Fisher, C1157) to produce stable intracellular carboxyfluorescein succinimidyl ester labeling (CFSE-PBMC). CFSE-PBMC were incubated for 3 days in RPMI 1640 medium supplemented with 5% FBS, 100 units/mL penicillin, 100 µg/mL streptomycin (Thermo Fisher, 15140122), and drug treatments (CRV431, CsA, or DMSO vehicle) in 96-well high protein-binding plates (275,000 cells per well) pre-coated with 2 µg/mL anti-CD3 antibody (UCHT clone) to cross-link lymphocyte CD3 T cell receptor and stimulate T cell division. Cells were collected after 3 days culture incubation, and flow cytometry was used to measure the partitioning of CFSE into daughter cells arising from cell division (discrete cell populations with successively halved CFSE content). Daughter cells as a percentage of all CFSE-labeled cells were normalized to DMSO treatment (100% stimulation) and wells without CD3 antibody coating (non-stimulated).

CRV431 Pharmacokinetics and Distribution

Male and female Sprague Dawley rats and male C57BL/6 mice from the carbon tetrachloride and NASH studies were used to evaluate CRV431 pharmacokinetics and distribution. CRV431 and CsA were dissolved in self-microemulsifying drug vehicles (Trepanier et al., 2018) and

JPET Fast Forward. Published on August 12, 2019 as DOI: 10.1124/jpet.119.261099
This article has not been copyedited and formatted. The final version may differ from this version.

administered by oral gavage. Terminal whole blood and livers were collected and frozen until drug extraction. Liver samples were homogenized in PBS or 1% formic acid (0.1 g – 0.4 g liver sample per ml solvent) with bead-based homogenizers (TissueLyser or Beadruptor). CRV431 and CsA concentration standards for sample quantitation were made by spiking the compounds into blood and liver matrices. Sample and standard compounds were extracted from blood and liver homogenates using a zinc sulfate/methanol precipitation method and quantified by liquid chromatography-electrospray ionization-mass spectrometry (LC-ESI-MS) by as previously described (Trepanier et al., 2018). Liver CRV431 concentrations were normalized to the masses of the liver samples.

Drug Transporter Inhibition

CRV431 inhibition of drug transporters was assessed by measuring the transport and/or accumulation of transporter substrate probes in three types of test systems (Supplementary Table 1). Briefly, PGP and BCRP inhibition was assessed by measuring the bidirectional transport of substrates across cell monolayers in transwell culture plates. Efflux ratios were represented as (apical-to-basal flux)/(basal-to-apical flux), and efflux ratios were plotted relative to CRV431 concentration to derive IC_{50} values. BSEP and MRP1 inhibition was assessed by measuring substrate accumulation in membrane vesicles prepared from insect Sf9 cells and recombinantly expressing BSEP and MRP2 (Genomembrane). Inhibition of all other transporters was assessed by measuring substrate accumulation in cells recombinantly expressing the transporter. Known inhibitors of each transporter were used as positive controls for the assays. CRV431 was tested at concentrations of 0.1, 0.3, 1, 3, 10, 30 and 50 µM. Specific, ATP-dependent uptake was determined by subtracting uptake in negative control vesicles and cells not expressing the transporters, and secondly by subtracting uptake in the absence of ATP in the assays. Specific, ATP-dependent uptake was plotted as a function of CRV431 concentrations and fitted to nonlinear regressions to obtain IC_{50} values.

JPET Fast Forward. Published on August 12, 2019 as DOI: 10.1124/jpet.119.261099
This article has not been copyedited and formatted. The final version may differ from this version.

Cytotoxicity Analysis

CRV431 cytotoxicity was evaluated in cell culture with 6 human cell types: Jurkat E6.1 lymphocyte cell line (Sigma, 88042803, male), HepaRG hepatocyte cell line (Life Technologies, HPRGC10, female), primary renal epithelial cells (Lonza, CC-2556, unknown gender), primary dermal fibroblasts (Lonza, CC-2511, female), primary bronchial smooth muscle cells (Lonza, CC-2576, male), and primary umbilical vein endothelial cells (Lonza, CC-2519, female). Jurkat cells (suspension cell type) were plated at 35,000 cells/well in 96-well plates. All other cell types (adherent cell types) were plated 2500 – 10,000 cells per well (adherent cell types) in GelCol bovine collagen-coated (Advanced Biomatrix, 5167) 96-well Nunc Edge 2.0 evaporation barrier plates (Thermo Scientific, 14387223). Cell culture medium and culture conditions followed suppliers' recommendations. Cultures were maintained for 3 days without medium change in the presence of DMSO drug vehicle, CsA, or CRV431 from 0.6 – 80 μM. The cell cultures demonstrated less than 50% confluency at plating and 90-100% confluency in DMSO control wells, indicating that cells were in a proliferation phase with little contact inhibition for most of the culture period. Cell viability was assessed at the end of the 3-day culture period using the In Vitro Toxicology Assay (Sigma, Tox8-1KT). In this assay the oxidoreduction indicator dye, resazurin, is colorometrically converted in proportion to the number of viable cells and measured by absorbance or fluorescence. Fluorescence was measured (excitation 540 nm; emission 590 nm) with a BMG Polarstar Galaxy Microplate Reader.

Mouse Studies

Experimental protocols were approved by the Institutional Animal Care and Use Committee of The Scripps Research Institute (La Jolla, CA) and adhered to guidelines from the National Institutes of Health (Bethesda, MD). Female pregnant E14 C57BL/6J mice were purchased from the Department of Animal Resource's Rodent Breeding Colony (The Scripps Research Institute;

La Jolla, CA), with pups used for experimentation. All mice were kept at the vivarium in The Scripps Research Institute's Department of Immunology & Microbiology (La Jolla, CA). Five mice were housed per cage with rolled newspaper as bedding and enriched with paper chunks for shredding and pultruded carbon tubes. Mice were maintained under a pathogen-free condition at 21°C with food and water provided *ad libitum* during daily cycles of twelve hours of light and darkness.

Carbon tetrachloride (CCl_4)-induced liver fibrosis was conducted in C57BL/6J male mice starting at 7 weeks of age. Mice were injected intraperitoneally twice per week with 0.5 to 0.75ml/kg CCL_4 (Sigma, 289116) and corn oil (0.05 ml total dose per mouse) for 6 weeks. CRV431, obeticholic acid (OCA; MedChemExpress, HY-12222), and vehicle were administered by daily oral gavage for the entire duration of the study. CRV431 and OCA were dissolved in a self-microemulsifying drug vehicle (Trepanier *et al.*, 2018), then diluted with PBS. CRV431 was administered at 50 mg/kg/day, and OCA was administered at 10 mg/kg/day.

Non-alcoholic steatohepatitis (NASH) was initiated in 2-day-old C57BL/6J male mice by intraperitoneal injection with 200 µg streptozotocin (Sigma, S0130) to disrupt pancreatic β cells, induce diabetes, and promote adiposity in the liver. Mice were weaned at 3 weeks of age and begun on a high fat diet (HFD) with 60%kcal fat (Research Diets Inc., D12492N) for the duration of the studies. Additionally, mice with a regular diet (Research Diets Inc., D12450KN) and without streptozotocin were included as negative controls. CRV431 was dissolved in a self-microemulsifying drug vehicle then diluted with PBS and administered daily by oral gavage at 50 mg/kg/day. The start time and duration of vehicle and CRV431 treatments varied depending on the study.

JPET Fast Forward. Published on August 12, 2019 as DOI: 10.1124/jpet.119.261099
This article has not been copyedited and formatted. The final version may differ from this version.

Blood and livers were collected at the end of the NASH and CCl_4 studies. In some studies, serum or plasma was isolated from freshly-collected blood, while in other studies blood was frozen for later analysis of CRV431 concentration. Livers were immersion-fixed in zinc-formalin and paraffin-embedded for histological processing. Liver sections were stained with hematoxylin and eosin for assessment of inflammation, ballooning, and steatosis, and with Sirius red for assessment of collagen I and III (fibrosis). Sirius red staining was quantified by blinded analysis in one section per liver using ImageJ software. Scoring of steatosis, ballooning, and inflammation (sum of portal and lobular inflammation) in liver sections was based on criteria and training by a board-certified pathologist. The following criteria were used for the histological scoring:

Score	Steatosis	Ballooning	Portal Inflammation	Lobular Inflammation
0	<5%	No ballooning	None/minimal	No foci
1	5-33%	Few balloon cells	Significant	<2 foci
2	33-66%	Many/prominent		2-4 foci
3	>66%			>4 foci

Liver tumors were quantified in freshly collected livers at sacrifice in one NASH study ending at 30 weeks of age. Liver tumors were counted and their diameters measured with a ruler and classified as small (>0.1 cm diameter but not exceeding 0.5 cm), medium (0.5 cm – 1 cm diameter), or large (>1 cm diameter). Liver tumor burden scores (0 – 7 scale) were assigned to each liver based on the following criteria:

Score	Description
0	no detectable tumor nodules
1	1-4 small nodules, and no medium or large nodules
2	more than 4 small nodules, and no medium or large nodules
3	unlimited number of small nodules, plus 1- 2 medium, and no large nodules
4	unlimited number of small nodules, plus 3 or more medium, and no large nodules
5	unlimited number of small and medium nodules but no more than 1 large nodule
6	unlimited number of small and medium nodules but no more than 2 large nodules
7	unlimited number of small and medium nodules, and 3 or more large nodules

RESULTS

CRV431 Potently Inhibits Multiple Cyclophilin Isoforms

Cyclophilin isomerase inhibition by CRV431 and CsA was assessed in a widely used enzymatic assay with recombinant cyclophilins (Kofron *et al.*, 1991). CRV431 and CsA inhibitory constants (Ki) towards cyclophilin A were determined by fitting substrate concentration-initial reaction velocity curves (multiple substrate concentrations) to the competitive enzyme inhibition model. These experiments yielded Ki values of 1.3 nM for CRV431 and 17.2 nM for CsA, indicating a 13-fold higher potency for CRV431. Maximum enzyme velocities (Vmax) in the presence of DMSO control, CRV431, or CsA were calculated to be 5.4, 5.3, and 4.7 µmol/sec/nmol Cyp A, respectively, with a mean value of 5.1 µmol/sec/nmol Cyp A. The similar Vmax values are consistent with the known competitive model of cyclophilin inhibition by cyclosporins (Fischer *et al.*, 1989). In the absence of inhibitor, the Km value was 0.94 µM.

Next, we evaluated CRV431 inhibition of three additional cyclophilin isoforms – B, D, and G (Table 1). These assays were performed with only one peptide substrate concentration, 160 µM, which therefore described CRV431 or CsA potencies as IC_{50} values. The measured IC_{50} values approximated the Ki values for Cyp A inhibition, indicating that IC_{50} values obtained in these assay conditions closely reflected the true inhibitory potencies of the compounds. Isomerase reactions performed with all the cyclophilin isoforms resulted in IC_{50} values of 2.5-7.3 nM for CRV431 and 10-28 nM for CsA (Table 1). Thus, cyclophilins A (PPIA), B (PPIB), D (PPIF), and G (PPIG) all were inhibited by CRV431 with low-nanomolar affinity, and CRV431 was 3.6 – 10.2-times more potent than CsA across all the isoforms.

JPET Fast Forward. Published on August 12, 2019 as DOI: 10.1124/jpet.119.261099
This article has not been copyedited and formatted. The final version may differ from this version.

CRV431 Demonstrates Low *in Vitro* Immunosuppressive Activity

Immunosuppression-related activity was assessed with two types of *in vitro* assay. The first type was Jurkat T lymphocytes stably transfected with luciferase reporter genes driven by one of two DNA promoter constructs. In one of the Jurkat lines the promoter construct was the binding sequence for human nuclear factor of activated T cells (NFAT), a transcription factor that is a primary calcineurin target and mediator of lymphocyte activation. In the second Jurkat line, the promoter construct was the interleukin-2 promoter which contains binding sequences for NFAT and two other transcription factors, NF-κB and AP-1. Both cell lines were stimulated for 18 hours in two ways: (a) addition of PMA + A23817 calcium ionophore, and; (b) incubation in culture plates pre-coated with antibodies to CD3 and CD28 to mimic physiological lymphocyte stimulation. Luciferase production and inhibition by CRV431 and CsA were nearly identical for both types of stimulation (Table 2 and Figure 1). CsA was able to completely suppress Jurkat activation with IC_{50} values ranging from 3-9 nM. CRV431 showed a shallower concentration-dependence inhibition curve and when tested up to 20 µM was not able to completely suppress activation. Nonlinear regression analysis gave CRV431 IC_{50} values ranging from 205-311 nM but estimates of 50% inhibition derived directly from the graphs were 340-500 nM. Based on the ratios of CRV431 and CsA IC_{50}'s, CRV431 was approximately 35-times less potent than CsA on Jurkat-IL-2 cells and 63-times less potent than CsA on Jurkat-NFAT cells, but these differences may be underestimates of CRV431's lower potency in these cells.

The second type of immunosuppression assay consisted of human PMBC that were stained with CFSE and cultured for 3 days with immobilized CD3 antibody to stimulate proliferation of the T cells. Cell proliferation was measured by flow cytometric quantitation of daughter cell populations with successively halved content of CFSE. CsA blocked lymphocyte proliferation with an IC_{50} of 59 nM, whereas CRV431 weakly inhibited proliferation. The highest tested CRV431 concentration of 10 µM inhibited proliferation by only 40%, which negated IC_{50}

determination. Also, the concentration-effect curve was very shallow, in similarity to the CRV431 effects in the Jurkat cell lines. Together, the data from these multiple assays indicate that CRV431 has significantly diminished immunosuppression potency which does not exceed 3% of CsA levels (35-fold difference).

CRV431 Demonstrates Lower Cytotoxicity Potential than CsA

CRV431 and CsA cytotoxicities were evaluated in 6 human cell types - Jurkat lymphocyte cell line, HepaRG hepatocyte cell line, primary renal epithelial cells, primary dermal fibroblasts, primary bronchial smooth muscle cells, and primary umbilical vein endothelial cells (Figure 2). Cell viability was measured after 3 days of culture and incubation with compounds up to 80 µM. CRV431 caused 100% lethality at the highest concentrations tested, and the mean CC_{50} was 23.6 µM. Maximum cytotoxicity of CsA was reached at 30 µM but did not reach 100% lethality in most experiments because CsA reached its limit of aqueous solubility at approximately 32 µM, as compared to CRV431's aqueous solubility of 115 µM (Trepanier et al., 2018). The mean CsA CC_{50} from all experiments was 12.6 µM, indicating that CRV431 had lower cytotoxicity potential than CsA.

Improved Drug Transporter Inhibition Profile for CRV431

Cyclosporins as a class are known to influence the pharmacokinetics of certain drugs and endogenous molecules by inhibiting their influx or efflux from cells through drug transporters. We therefore investigated inhibition of a panel of transporters by CRV431 in comparison to CsA. Three types of test systems were used – membrane-derived vesicles, conventional cell cultures, and transwell cultures (Table 3). Each test system expressed an individual transporter, and data were validated by comparison to vesicles and cells without the transfected transporter and by use of known transporter inhibitors as positive controls. Four transporters were not inhibited by CsA or CRV431 at the highest tested concentration of 50 µM – OAT1, OCT2, MATE-1, MATE-2.

JPET Fast Forward. Published on August 12, 2019 as DOI: 10.1124/jpet.119.261099
This article has not been copyedited and formatted. The final version may differ from this version.

Only one transporter, OAT1, was inhibited by CRV431 more potently than CsA, with a 21-times lower IC_{50}. CRV431 showed a small advantage over CsA towards BSEP and MRP2, demonstrating 2-3-fold higher IC_{50} values, and a more significant advantage towards BCRP, OATP1B1, and OATP1B3, with approximately 7-fold higher IC_{50} than CsA. The most significant advantage of CRV431 was towards NTCP and P-gp (MDR1) where the CRV431 IC_{50} was 45-50-times higher than the CsA IC_{50}. These data show that CRV431 is less inhibitory than CsA towards most membrane transporters and predict that CRV431 should have few drug-drug interactions and less impact on the transport of endogenous molecules such as bile salts and bilirubin.

CRV431 Absorption and Distribution

CRV431 blood and liver exposures following daily oral dosing were evaluated in several mouse and rat studies (Table 4). Across a large range of doses, 30-250 mg/kg/day, and dosing periods, 7–189 days, blood levels of CRV431 were consistently around 1-3 µg/ml. This was also observed across a wide range of sampling periods from 3–24 hr post-dose, suggesting a long half-life for CRV431. We also consistently observed much higher concentrations in livers, representing 5-15-fold higher levels than in the blood. High liver exposures may suggest pharmacokinetics of CRV431 favor hepatic delivery or targeting of CRV431. Mice from NASH and carbon tetrachloride models of disease had higher liver-to-blood ratios of CRV431 than normal rats.

A more detailed pharmacokinetic analysis in normal rats following a single oral dose confirmed a relatively long CRV431 half-life which exceeded that of CsA (Figure 4). This was also exemplified by clearance values (CL/F) of 0.32 mL/min/kg for CRV431 and 1.11 for CsA, representing a 3.5-fold difference. CRV431 peak blood concentrations (Cmax) and $AUC_{0\text{-}24\ hr}$

JPET Fast Forward. Published on August 12, 2019 as DOI: 10.1124/jpet.119.261099
This article has not been copyedited and formatted. The final version may differ from this version.

exceeded those of CsA by a factor of 1.6 and 2.2 respectively, which may be due to differences in oral bioavailability and/or drug clearance.

CRV431 in the Carbon Tetrachloride Mouse Model of Liver Fibrosis

The high levels of CRV431 in livers, inhibition of multiple cyclophilins, and other favorable properties described above suggested that CRV431 may be a good candidate for testing in liver disease models. One common model is chronic dosing of mice with the hepatotoxin, carbon tetrachloride (CCl_4), which leads primarily to liver fibrosis. C57BL/6 male mice were dosed twice weekly with CCl_4 for 6 weeks with daily oral dosing of vehicle or CRV431 (50 mg/kg/day). Obeticholic acid (OCA), a compound in development as a NASH treatment, was included as a comparator compound and dosed at 10 mg/kg/day. CCl_4 induced liver fibrosis, as demonstrated by 10-fold higher levels of collagen staining with Sirius Red in liver sections as compared to mice not administered CCl_4 (Figure 4). CRV431 treatment lowered the amount of Sirius Red staining by 43%, in contrast to OCA which had no statistically significant effect. One group of CCl_4 mice that were treated with a combination of CRV431 and OCA also showed fibrosis reduction to similar levels as CRV431 alone.

CRV431 in a Mouse NASH Model

The second mouse model used to evaluate CRV431 efficacy was a NASH model in which C57BL/6 mice were given a single dose of streptozotocin at 2 days old and a high-fat diet starting at 3 weeks of age. Mice progressively developed obesity, liver steatosis, fibrosis, and eventually liver tumors starting beyond 14 weeks of age. Three separate studies were conducted in this model, varying in the start time and duration of CRV431 treatment. In similarity to the CCl_4 study we found that daily oral treatment with CRV431 at 50 mg/kg/day decreased the level of fibrosis in all three NASH model studies as determined by Sirius Red staining of liver sections (Table 5 and Figure 5). CRV431 was effective when administered either at early-to-

intermediate stages of the model (i.e. Weeks 3-14 and Weeks 8-14 treatment), or at late stage of the model (i.e. Week 20-30 treatment). Fibrosis levels were 37 – 46% lower after CRV431 treatment compared to vehicle treatment. Statistically significant differences between vehicle and CRV431 treatment groups were also observed for body weight and NASH activity score (NAS) score (composite of steatosis, inflammation, and ballooning) in the Week 3-14 treatment study. In the Week 20-30 treatment study, fibrosis scores from the CRV431-treated mice were lower than for the vehicle-treated mice.

Mouse livers examined at Week 14 had no tumors, whereas vehicle-treated mice at Week 30 had an extensive tumor load, indicating that liver tumors developed sometime during Weeks 14-30 (Figure 6). Histopathological assessment indicated that the tumors were cellular in nature and therefore likely represented hepatocellular carcinoma. Moreover, in the vehicle control group all mice had liver tumors, and 3 of 10 livers had nodules that were 1 cm or larger in diameter. In contrast, CRV431 treatment from Week 20-30 resulted in half the number of tumors, with smaller tumors on average, with 2 of 10 livers of CRV431-treated mice lacking tumors. A scoring system reflecting a combination of tumor number and size revealed that CRV431 decreased the tumor burden by 52%. Further studies are required to determine if the reduced tumor load is mechanistically linked to the lower fibrosis levels or reflects a more direct effect on the cells.

DISCUSSION

Experimental and clinical evidence has accumulated over nearly 3 decades indicating that antagonists of cyclophilins may offer clinical benefits. Many attempts have been made to develop cyclophilin inhibitors for clinical use, the most notable being alisporivir (Debio-025) which demonstrated good antiviral activity toward hepatitis C virus (Buti *et al.*, 2015; Pawlotsky *et al.*, 2015). However, all cyclophilin-inhibiting drug candidates eventually faced obstacles that halted their development. CsA was the original and still the only approved drug that inhibits cyclophilins, but its immunosuppressive activity limits its clinical use for indications other than transplantation and autoimmune diseases. Our testing showed that CRV431 has greatly diminished immunosuppression potency, high cyclophilin inhibition potency, and other properties that are favorable for clinical development for liver diseases.

CRV431 inhibited the isomerase activity of cyclophilins A, B, D, and G. However, CRV431 probably also blocks several other isoforms based on conservation of the active sites and by the observation that CsA binds to at least 11 of the 18 reported isoforms (Davis *et al.*, 2010; Lavin and McGee, 2015). The pan-inhibitory activity is proposed to be advantageous since a single drug could simultaneously target multiple pathological activities and minimize the risk, complications, and expense of combining multiple, single-pathway drugs. Anti-inflammatory, anti-cancer, and anti-viral activities have been linked to Cyp A inhibition (Yurchenko *et al.*, 2010; Tian-Tian *et al.*, 2013; Lavin and McGee, 2015; Dawar *et al.*, 2017). Anti-fibrotic activities may be linked to Cyp B inhibition due to its role in collagen production (Choi *et al.*, 2009; Cabral *et al.*, 2014; Terajima *et al.*, 2016; Gjaltema and Bank, 2017). Cytoprotective properties are linked to Cyp D inhibition and desensitization of mitochondrial permeability transition (Alam *et al.*, 2015; Springer *et al.*, 2015; Porter and Beutner, 2018). Targeting multiple pathways is likely a

prerequisite for effectively treating chronic inflammatory and fibrotic diseases, and cyclophilin inhibition may be one way of achieving this goal.

Cyclophilins are abundant in eukaryotic cells and have important physiological functions, so questioning their suitability as drug targets is reasonable. Genetic knockouts of individual isoforms A, B, and D in mice are generally well-tolerated, and in fact most studies document positive effects of cyclophilin knockout in disease models (Nigro *et al.*, 2011; Elvers *et al.*, 2012; Guo *et al.*, 2016; Shum *et al.*, 2016; Huang *et al.*, 2017; Wang *et al.*, 2018). More informative than genetic knockouts are the 35 years of clinical experience with CsA and its analogs. Although CsA can exhibit side effects such as nephrotoxicity, hypertension, and dyslipidemia, it can be taken life-long by organ transplant patients under careful management. Moreover, many of the side effects appear to result from its immunosuppressive activity rather than cyclophilin binding. Firstly, some of the clinical toxicities of CsA also occur with another calcineurin inhibitor, tacrolimus, which does not bind to cyclophilins. Secondly, the nonimmunosuppressive analog, alisporivir, was dosed to over 2000 patients at high doses and showed no renal toxicity or infections characteristic of CsA treatment and a moderation of other CsA-like side effects (Buti *et al.*, 2015; Pawlotsky *et al.*, 2015; Zeuzem *et al.*, 2015; Stanciu *et al.*, 2019). Finally, preclinical toxicology studies with CRV431 showed a remarkably good safety profile which has enabled clinical studies.

Several findings point to advantages of CRV431 over CsA and other previously described cyclophilin inhibitors. Firstly, CRV431 is not expected to exhibit clinically significant immunosuppression, based on *in vitro* assays that showed at least 35-fold less immunosuppressive activity than CsA and based on our observations that CRV431 efficacy occurred in mice at peak blood levels of 1.2-1.4 µg/ml which is only slightly higher than the therapeutic range for CsA in transplantation – peak levels of 0.45-1.3 µg/ml and trough levels of

0.1-0.35 µg/ml (BC Transplant Provincial Health Services Authority, 2019). Secondly, the lower cytotoxicity potency of CRV431 means that there is less likelihood of side effects arising from excessive drug accumulation in organs. Thirdly, CRV431 is predicted to have few drug-drug interactions or toxicities arising from membrane transporter inhibition, based on our *in vitro* profiling. Interestingly, CRV431 possesses similar physicochemical characteristics to those identified by Novartis as being critical for minimizing transporter inhibition by cyclosporins, which represent a significant improvement over alisporivir and CsA (Fu *et al.*, 2014). Cyclosporine inhibition of several membrane transporters can affect the clinical disposition of other compounds, and CRV431 was non-inhibitory or less potent than CsA towards all of them, with the exception of OAT3. The most notable transporter findings were the absence of P-gp inhibition in the Caco-2 transwell assay and the 45-fold lower activity towards the bile salt transporter, NTCP. A transporter of conjugated bilirubin, MRP2, also was slightly less affected by CRV431 than CsA. These latter findings suggest that CRV431 is less likely to impact bilirubin and bile salt transport, and results from preclinical toxicology studies are consistent with this prediction. Despite these positive *in vitro* and preclinical findings, it will be important to monitor patients for drug-drug interactions considering the effects that CsA are known to exhibit. One final advantage of CRV431 as a drug candidate for liver disease is that its steady-state accumulation in the liver, the intended site of action, was 5-15-fold higher than in the blood. This characteristic, however, is not unique to CRV431, as CsA also preferentially localizes to the liver (Wagner et al. 1987; Lensmeyer *et al.*, 1991).

The decreased liver fibrosis observed in 4 studies with 2 mouse models are consistent with several previous studies that used CsA or other nonimmunosuppressive analogs. CsA and NIM811 administered to CCl_4-treated rats lowered liver fibrosis, ALT, inflammation, TGFβ, TIMP-1 and other markers (Lie et al., 1991; Wang et al., 2011). In the rat bile duct ligation model NIM811 did not reduce fibrosis but decreased liver necrosis and ALT (Rehman *et al.*,

2008). In a clinical study of liver transplantation that compared CsA to tacrolimus, less post-transplant liver fibrosis was observed in steroid-free, CsA-treated patients (Levy *et al.*, 2014). Anti-fibrotic effects have also been observed with NIM811 and MM284 in models of cardiac fibrosis (Seizer *et al.*, 2012; Heinzmann *et al.*, 2015). The physicochemical properties of MM284 dictate that it targets extracellular cyclophilins, which suggests that fibrosis is lowered at least partly by attenuating Cyp A-CD147-mediated inflammation (Iordanskaia *et al.*, 2015). Similarly, in the unilateral ureter obstruction model, preservation of cell viability and lowering of inflammation by Cyp D knockout partly prevents renal fibrosis (Hou *et al.*, 2018). Direct, anti-fibrotic effects on hepatic stellate cells, the primary cell type implicated in liver fibrosis, is another proposed mode of action. CsA, NIM811, and SCY-635 alter many activities in these cells in culture towards an anti-fibrotic phenotype, including changes in collagen production, MMP and TIMP-1 levels, and TGFβ and MAPK signaling pathways (Nakamuta *et al.*, 2005; Kohjima *et al.*, 2007; Scorneaux *et al.*, 2010). Future studies will attempt to identify the contributions of each cyclophilin isoform and their modes of action in liver fibrosis.

The significant reduction in tumor number and size by CRV431 in the NASH mouse model was supported by previous reports suggesting numerous possible mechanisms. The reduction in fibrosis may have limited tumor growth, since hepatocellular carcinoma is regulated strongly by the extracellular milieu (Cox and Erler, 2014; Baglieri *et al.*, 2019; Sircana *et al.*, 2019). CRV431 may have restored levels or function of the tumor suppressor, p53, by blocking the binding of Cyp D to p53 or blocking p53 degradation through a Cyp A-mediated mechanism (Bigi *et al.*, 2016; Lu *et al.*, 2017). Cancer cells frequently express high levels of cyclophilins which appears to support the elevated anabolic demands, cell proliferation, and hypoxia adaptations of the cells. For example, the transcription factor, hypoxia-inducible factor-1, binds to the Cyp A and B promoters and upregulates cyclophilin production (Kim *et al.*, 2011; Zhang *et al.*, 2014). A nuclear cyclophilin isoform, cyclophilin J, is upregulated in many hepatocellular carcinomas and

facilitates cell cycle progression in part through cyclin D1 elevation (Chen *et al.*, 2015). Extracellular Cyp A can increase cholangiocarcinoma cell proliferation through binding to CD147 receptor (Obchoei *et al.*, 2015). Conversely, decreasing cyclophilins or blocking their function has been shown to suppress cancer cell proliferation and metastasis (Kim *et al.*, 2011; Zhang *et al.*, 2011, 2014; Choi *et al.*, 2014, 2018; Brichkina *et al.*, 2016; Guo *et al.*, 2018). Thus, CRV431 may lower the risk of hepatocellular carcinoma not only indirectly by helping to normalize the liver parenchyma but also directly by suppressing cell proliferation or adaptive intracellular pathways required for carcinogenesis.

In conclusion, many investigators have identified the need and therapeutic opportunities of a potent cyclophilin inhibitor without the immunosuppression and other liabilities of CsA. Findings from the present study and previous studies endorse CRV431 as the strongest candidate to date to fulfill this role. Its ability to attenuate multiple pathological and viral activities and its inherent disposition to the liver makes CRV431 particularly well suited for liver diseases of various etiologies. A single drug that could decrease both liver fibrosis and cancer incidence would be valuable asset in the management of non-alcoholic, alcoholic, and viral hepatitis.

AUTHORSHIP CONTRIBUTIONS

Participated in research design: Kuo, Ure, Trepanier, Gallay, Foster

Conducted experiments: Kuo, Ure, Bobardt, Chatterjji

Performed data analysis: Kuo, Ure, Gallay, Trepanier, Mayo

Contributed to the writing of the manuscript: Kuo, Ure, Trepanier, Mayo, Gallay, Foster

REFERENCES

Alam MR, Baetz D, and Ovize M (2015) Cyclophilin D and myocardial ischemia-reperfusion injury: A fresh perspective. *J Mol Cell Cardiol* **78**:80–89.

Baglieri J, Brenner DA, and Kisseleva T (2019) The role of fibrosis and liver-associated fibroblasts in the pathogenesis of hepatocellular carcinoma. *Int J Mol Sci* **20**:E1723.

BC Transplant Provincial Health Services Authority (2019) *BC CLINICAL GUIDELINES FOR Transplant Medications*.

Bigi A, Beltrami E, Trinei M, Stendardo M, Pelicci PG, and Giorgio M (2016) Cyclophilin D counteracts P53-mediated growth arrest and promotes Ras tumorigenesis. *Oncogene* **35**:5132–5143.

Brichkina A, Nguyen NTM, Baskar R, Wee S, Gunaratne J, Robinson RC, and Bulavin D V. (2016) Proline isomerisation as a novel regulatory mechanism for p38MAPK activation and functions. *Cell Death Differ* **23**:1592–1601.

Briston T, Selwood DL, Szabadkai G, and Duchen MR (2019) Mitochondrial Permeability Transition: A Molecular Lesion with Multiple Drug Targets. *Trends Pharmacol Sci* **40**:50–70.

Buti M, Flisiak R, Kao JH, Chuang WL, Streinu-Cercel A, Tabak F, Calistru P, Goeser T, Rasenack J, Horban A, Davis GL, Alberti A, Mazzella G, Pol S, Orsenigo R, and Brass C (2015) Alisporivir with peginterferon/ribavirin in patients with chronic hepatitis C genotype 1 infection who failed to respond to or relapsed after prior interferon-based therapy: FUNDAMENTAL, a Phase II trial. *J Viral Hepat* **22**:596–606.

Cabral WA, Perdivara I, Weis MA, Terajima M, Blissett AR, Chang W, Perosky JE, Makareeva EN, Mertz EL, Leikin S, Tomer KB, Kozloff KM, Eyre DR, Yamauchi M, and Marini JC (2014) Abnormal Type I Collagen Post-translational Modification and Crosslinking in a Cyclophilin B KO Mouse Model of Recessive Osteogenesis Imperfecta. *PLoS Genet*

10:e1004465.

Chen J, Chen S, Wang J, Zhang M, Gong Z, Wei Y, Li L, Zhang Y, Zhao X, Jiang S, and Yu L (2015) Cyclophilin J is a novel peptidyl-prolyl isomerase and target for repressing the growth of hepatocellular carcinoma. *PLoS One* **10**: e0127668 .

Choi JW, Schroeder MA, Sarkaria JN, and Bram RJ (2014) Cyclophilin B supports MYC and mutant p53-dependent survival of glioblastoma multiforme cells. *Cancer Res* **74**:484–496.

Choi JW, Sutor SL, Lindquist L, Evans GL, Madden BJ, Bergen HR, Hefferan TE, Yaszemski MJ, and Bram RJ (2009) Severe osteogenesis imperfecta in cyclophilin B-deficient mice. *PLoS Genet* **5**:e1000750.

Choi TG, Nguyen MN, Kim J, Jo YH, Jang M, Nguyen NNY, Yun HR, Choe W, Kang I, Ha J, Tang DG, and Kim SS (2018) Cyclophilin B induces chemoresistance by degrading wild-type p53 via interaction with MDM2 in colorectal cancer. *J Pathol* **246**:115–126.

Cox TR, and Erler JT (2014) Molecular pathways: Connecting fibrosis and solid tumor metastasis. *Clin Cancer Res* **20**:3637–3643.

Davis TL, Walker JR, Campagna-Slater V, Finerty PJ, Finerty PJ, Paramanathan R, Bernstein G, Mackenzie F, Tempel W, Ouyang H, Lee WH, Eisenmesser EZ, and Dhe-Paganon S (2010) Structural and biochemical characterization of the human cyclophilin family of peptidyl-prolyl isomerases. *PLoS Biol* **8**:e1000439.

Dawar FU, Wu J, Zhao L, Khattak MNK, Mei J, and Lin L (2017) Updates in understanding the role of cyclophilin A in leukocyte chemotaxis. *J Leukoc Biol* **101**:823–826.

Dunyak B, and Gestwicki J (2016) Peptidyl-Proline Isomerases (PPIases): Targets for Natural Products and Natural Product-Inspired Compounds. *J Med Virol* **59**:9622–9644.

Elvers M, Herrmann A, Seizer P, Münzer P, Beck S, Schönberger T, Borst O, Martin-Romero FJ, Lang F, May AE, and Gawaz M (2012) Intracellular cyclophilin A is an important Ca 2+ regulator in platelets and critically involved in arterial thrombus formation. *Blood* **120**:1317–1326.

Fischer G, Wittmann-liebold B, Lang K, Kiefhaber T, and Schmid FX (1989) Cyclophilin and peptidyl-prolyl cis-trans isomerase are probably identical proteins. *Nature* **337**:476–478.

Fu J, Tjandra M, Becker C, Bednarczyk D, Capparelli M, Elling R, Hanna I, Fujimoto R, Furegati M, Karur S, Kasprzyk T, Knapp M, Leung K, Li X, Lu P, Mergo W, Miault C, Ng S, Parker D, Peng Y, Roggo S, Rivkin A, Simmons RL, Wang M, Wiedmann B, Weiss AH, Xiao L, Xie L, Xu W, Yifru A, Yang S, Zhou B, and Sweeney ZK (2014) Potent nonimmunosuppressive cyclophilin inhibitors with improved pharmaceutical properties and decreased transporter inhibition. *J Med Chem* **57**: 8503-8516.

Gallay PA, Bobardt MD, Chatterji U, Trepanier DJ, Ure D, Ordonez C, and Foster R (2015) The novel cyclophilin inhibitor CPI-431-32 concurrently blocks HCV and HIV-1 infections via a similar mechanism of action. *PLoS One* **10**: e0134707.

Gallay PP, Ure D, Bobardt M, Chatterji U, Ou J, Trepanier D, and Foster R (2019) The cyclophilin inhibitor CRV431 inhibits liver HBV DNA and HBsAg in transgenic mice. *PLoS One* **14**: e0217433.

Gjaltema RAF, and Bank RA (2017) Molecular insights into prolyl and lysyl hydroxylation of fibrillar collagens in health and disease. *Crit Rev Biochem Mol Biol* **52**:74–95.

Guo M, James AW, Kwak JH, Shen J, Yokoyama KK, Ting K, Soo CB, and Chiu RH (2016) Cyclophilin A (CypA) Plays Dual Roles in Regulation of Bone Anabolism and Resorption. *Sci Rep* **6**:2–11.

Guo Y, Jiang M, Zhao X, Gu M, Wang Z, Xu S, and Yue W (2018) Cyclophilin A promotes non-small cell lung cancer metastasis via p38 MAPK. *Thorac Cancer* **9**:120–128.

Heinzmann D, Bangert A, Müller AM, Von Ungern-Sternberg SNI, Emschermann F, Schönberger T, Chatterjee M, Mack AF, Klingel K, Kandolf R, Malesevic M, Borst O, Gawaz M, Langer HF, Katus H, Fischer G, May AE, Kaya Z, and Seizer P (2015) The novel extracellular Cyclophilin A (CyPA) - Inhibitor MM284 reduces myocardial inflammation and remodeling in a mouse model of troponin I -induced myocarditis.

Hou W, Leong KG, Ozols E, Tesch GH, Nikolic-Paterson DJ, and Ma FY (2018) Cyclophilin D promotes tubular cell damage and the development of interstitial fibrosis in the obstructed kidney. *Clin Exp Pharmacol Physiol* **45**:250–260.

Huang ZL, Pandya D, Banta DK, Ansari MS, and Oh U (2017) Cyclophilin inhibitor NIM811 ameliorates experimental allergic encephalomyelitis. *J Neuroimmunol* **311**:40–48.

Iordanskaia T, Malesevic M, Fischer G, Pushkarsky T, Bukrinsky M, and Nadler EP (2015) Targeting Extracellular Cyclophilins Ameliorates Disease Progression in Experimental Biliary Atresia. *Mol Med* **21**:657–664.

Kim Y, Jang M, Lim S, Won H, Yoon KS, Park JH, Kim HJ, Kim BH, Park WS, Ha J, and Kim SS (2011) Role of cyclophilin B in tumorigenesis and cisplatin resistance in hepatocellular carcinoma in humans. *Hepatology* **54**:1661–1678.

Kofron JL, Kuzmič P, Kishore V, Rich DH, and Colón-Bonilla E (1991) Determination of Kinetic Constants for Peptidyl Prolyl Cis-Trans Isomerases by an Improved Spectrophotometric Assay. *Biochemistry* **30**:6127–6134.

Kohjima M, Enjoji M, Higuchi N, Kotoh K, Kato M, Takayanagi R, and Nakamuta M (2007) NIM811, a nonimmunosuppressive cyclosporine analogue, suppresses collagen production and enhances collagenase activity in hepatic stellate cells. *Liver Int* **27**:1273–1281.

Kulik L, and El-Serag HB (2019) Epidemiology and Management of Hepatocellular Carcinoma. *Gastroenterology* **156**:477-491.

Lavin P, and McGee M (2015) Cyclophilin function in Cancer; lessons from virus replication. *Curr Mol Pharmacol* **9**:148–164.

Lensmeyer GL, Wiebe DA, Carlson IH, and Subramanian R (1991) Concentrations of cyclosporin A and its metabolites in human tissues postmortem. *J Anal Toxicol* **15**:110–115.

Levy G, Villamil FG, Nevens F, Metselaar HJ, Clavien P-A, Klintmalm G, Jones R, Migliaccio M, Prestele H, and Orsenigo R (2014) REFINE: A Randomized Trial Comparing Cyclosporine

A and Tacrolimus on Fibrosis After Liver Transplantation for Hepatitis C. *Am J Transplant* **14**:635–646.

Lie TS, Preissinger H, Bach M, Vogel J, Ogawa K, Kroeger T, and Brunner G (1991) The protective effect of cyclosporine against cirrhotic alteration of the liver. *Surgery* **110**:847–53.

Lu W, Cheng F, Yan W, Li X, Yao X, Song W, Liu M, Shen X, Jiang H, Chen J, Li J, and Huang J (2017) Selective targeting p53WT lung cancer cells harboring homozygous p53 Arg72 by an inhibitor of CypA. *Oncogene* **36**:4719–4731.

Moss SJ, Bobardt M, Leyssen P, Coates N, Chatterji U, Dejian X, Foster T, Liu J, Nur-e-Alam M, Suthar D, Yongsheng C, Warneck T, Zhang M-Q, Neyts J, Gallay P, Wilkinson B, and Gregory MA (2012) Sangamides, a new class of cyclophilin-inhibiting host-targeted antivirals for treatment of HCV infection. *Medchemcomm* **3**:938–943.

Nakamuta M, Kohjima M, Fukushima M, Morizono S, Kotoh K, Kobayashi N, and Enjoji M (2005) Cyclosporine suppresses cell growth and collagen production in hepatic stellate cells. *Transplant Proc* **37**:4598–4602.

Naoumov N V. (2014) Cyclophilin inhibition as potential therapy for liver diseases. *J Hepatol* **61**:1166–1174.

Nigro P, Pompilio G, and Capogrossi MC (2013) Cyclophilin A: A key player for human disease. *Cell Death Dis* **4**:e888-10.

Nigro P, Satoh K, O'Dell MR, Soe NN, Cui Z, Mohan A, Abe J, Alexis JD, Sparks JD, and Berk BC (2011) Cyclophilin A is an inflammatory mediator that promotes atherosclerosis in apolipoprotein E–deficient mice. *J Exp Med* **208**:53–66.

Obchoei S, Sawanyawisuth K, Wongkham C, Kasinrerk W, Yao Q, Chen C, and Wongkham S (2015) Secreted cyclophilin A mediates G1/S phase transition of cholangiocarcinoma cells via CD147/ERK1/2 pathway. *Tumor Biol* **36**:849–859.

Pawlotsky J-MM, Flisiak R, Sarin SK, Rasenack J, Piratvisuth T, Chuang W-LL, Peng C-YY,

Foster GR, Shah S, Wedemeyer H, Hézode C, Zhang W, Wong KA, Li B, Avila C, and Naoumov N V. (2015) Alisporivir plus ribavirin, interferon free or in combination with pegylated interferon, for hepatitis C virus genotype 2 or 3 infection. *Hepatology* **62**:1013–1023.

Porter GA, and Beutner G (2018) Cyclophilin D, Somehow a Master Regulator of Mitochondrial Function. *Biomolecules* **8**:176.

Rehman H, Ramshesh VK, Theruvath TP, Kim I, Currin RT, Giri S, Lemasters JJ, and Zhong Z (2008) NIM811 (N-Methyl-4-isoleucine Cyclosporine), a Mitochondrial Permeability Transition Inhibitor, Attenuates Cholestatic Liver Injury but Not Fibrosis in Mice. *J Pharmacol Exp Ther* **327**:699–706.

Scorneaux B, Thomas G, Hopkins S, and Harris R (2010) The effects of SCY-635, a nonimmunosuppressive cyclosporine analog on stellate cell proliferation, collagen synthesis, TIMP-1 and collagenase production. *Hepatology* **52**:183.

Seizer P, Klingel K, Sauter M, Westermann D, Ochmann C, Schönberger T, Schleicher R, Stellos K, Schmidt EM, Borst O, Bigalke B, Kandolf R, Langer H, Gawaz M, and May AE (2012) Cyclophilin A affects inflammation, virus elimination and myocardial fibrosis in coxsackievirus B3-induced myocarditis. *J Mol Cell Cardiol* **53**:6–14.

Shum LC, White NS, Nadtochiy SM, De Mesy Bentley KL, Brookes PS, HJonason J, and Eliseev RA (2016) Cyclophilin D Knock-out mice show enhanced resistance to osteoporosis and to metabolic changes observed in aging bone. *PLoS One* **11**:1–18.

Sircana A, Paschetta E, Saba F, Molinaro F, and Musso G (2019) Recent Insight into the Role of Fibrosis in Nonalcoholic Steatohepatitis-Related Hepatocellular Carcinoma. *Int J Mol Sci* **20**:1745.

Springer JE, Prajapati P, and Sullivan PG (2015) Targeting the mitochondrial permeability transition pore in traumatic central nervous system injury. *Neural Regen Res* **13**:1338–1341.

Stanciu C, Trifan A, Muzica C, and Sfarti C (2019) Efficacy and safety of alisporivir for the treatment of hepatitis C infection. *Expert Opin Pharmacother* **20**:379–384.

Sweeney ZK, Fu J, and Wiedmann B (2014) From chemical tools to clinical medicines: Nonimmunosuppressive cyclophilin inhibitors derived from the cyclosporin and sanglifehrin scaffolds. *J Med Chem* **57**: 7145-7159

Terajima M, Taga Y, Chen Y, Cabral WA, Hou-Fu G, Srisawasdi S, Nagasawa M, Sumida N, Hattori S, Kurie JM, Marini JC, and Yamauchi M (2016) Cyclophilin-B modulates collagen cross-linking by differentially affecting lysine hydroxylation in the helical and telopeptidyl domains of tendon type I collagen. *J Biol Chem* **291**: 9501-9512.

Tian-Tian Z, Jun-Feng Z, and Heng G (2013) Functions of cyclophilin A in atherosclerosis. *Exp Clin Cardiol* **18**:e118-24.

Trepanier DJ, Ure DR, and Foster RT (2018) Development, characterization, and pharmacokinetic evaluation of a crv431 loaded self-microemulsifying drug delivery system. *J Pharm Pharm Sci* **21**:335s-348s.

Ullah Dawar F, Tu J, Nasir Khan Khattak M, Mei J, and Lin L (2017) Cyclophilin A: A Key Factor in Virus Replication and Potential Target for Anti-viral Therapy. *Curr Issues Mol Biol* **21**:1–20.

Wagner, O., Schreier, E., Heitz, F., Maurer G (1987) Tissue Distribution, Disposition, and Metabolism of Cyclosporine in Rats. *Drug Metab Dispos* **15**:377–383.

Wang H, Zhang Y, Wang T, You H, and Jia J (2011) N-methyl-4-isoleucine cyclosporine attenuates CCl 4 -induced liver fibrosis in rats by interacting with cyclophilin B and D. *J Gastroenterol Hepatol* **26**:558–567.

Wang X, Du H, Shao S, Bo T, Yu C, Chen W, Zhao L, Li Q, Wang L, Liu X, Su X, Sun M, Song Y, Gao L, and Zhao J (2018) Cyclophilin D deficiency attenuates mitochondrial perturbation and ameliorates hepatic steatosis. *Hepatology* **68**:62–77.

Xue C, Sowden MP, and Berk BC (2018) Extracellular and intracellular cyclophilin A, native and

post-translationally modified, show diverse and specific pathological roles in diseases. *Arterioscler Thromb Vasc Biol* **38**:986–993.

Yan W, Qing J, Mei H, Mao F, Huang J, Zhu J, Jiang H, Liu L, Zhang L, and Li J (2015) Discovery of novel small molecule anti-HCV agents via the CypA inhibitory mechanism using o-acylation-directed lead optimization. *Molecules* **20**:10342-10359.

Yurchenko V, Constant S, Eisenmesser E, and Bukrinsky M (2010) Cyclophilin-CD147 interactions: A new target for anti-inflammatory therapeutics. *Clin Exp Immunol* **160**:305–317.

Zeuzem S, Flisiak R, Vierling JM, Mazur W, Mazzella G, Thongsawat S, Abdurakhmanov D, Van Kính N, Calistru P, Heo J, Stanciu C, Gould M, Makara M, Hsu SJ, Buggisch P, Samuel D, Mutimer D, Nault B, Merz M, Bao W, Griffel LH, Brass C, and Naoumov N V. (2015) Randomised clinical trial: Alisporivir combined with peginterferon and ribavirin in treatment-naïve patients with chronic HCV genotype 1 infection (ESSENTIAL II). *Aliment Pharmacol Ther* **42**:829–844.

Zhang H, Chen J, Liu F, Gao C, Wang X, Zhao T, Liu J, Gao S, Zhao X, Ren H, and Hao J (2014) CypA, a gene downstream of HIF-1α, promotes the development of PDAC. *PLoS One* **9**:e92824.

Zhang M, Dai C, Zhu H, Chen S, Wu Y, Li Q, Zeng X, Wang W, Zuo J, Zhou M, Xia Z, Ji G, Saiyin H, Qin L, and Yu L (2011) Cyclophilin A promotes human hepatocellular carcinoma cell metastasis via regulation of MMP3 and MMP9. *Mol Cell Biochem* **357**:387–395.

FOOTNOTES

This work was supported by the National Institutes of Health National Institute of Allergy and Infectious Diseases under award number AI125365 (J.K., M.B., U.C. and P.G.). Joseph Kuo is supported by the Ruth L. Kirschstein Institutional National Research Service Award (T32AI007244) at The Scripps Research Institute, sponsored by the National Institutes of Health National Institute of Allergy and Infectious Diseases. Partial support for the project also was provided by Contravir Pharmaceuticals Inc..

Portions of this work were presented previously:

American Association for the Study of the Liver (AASLD) 2018 Liver Meeting, *Hepatology* Volume 68, Issue S1, Abstract #418. Title: CRV431, a Cyclophilin Inhibitor, Reduces Fibrosis and Tumor Burden in Mice with Hepatocellular Carcinoma

JPET Fast Forward. Published on August 12, 2019 as DOI: 10.1124/jpet.119.261099
This article has not been copyedited and formatted. The final version may differ from this version.

FIGURE LEGENDS

Figure 1. *In vitro* immunosuppression-related assays

(A and B) Jurkat T cells stably transfected with a luciferase reporter driven by NFAT or IL-2 promoter were stimulated with PMA and A23187 calcium ionophore (A) or immobilized CD3 and CD28 antibodies (B) in the presence of CRV431, CsA, or DMSO vehicle. Luciferase expression was measured after 18 hr stimulation. (C) Human peripheral blood mononuclear cells were labeled with CFSE and stimulated for 3 days by incubation with immobilized CD3 antibody in the presence of CRV431, CsA, or DMSO vehicle. The percentage of cells that underwent cell division after 3 days was determined by flow cytometric measurement of CFSE partitioning to daughter cells. Means and standard deviations shown (N = 2-3 replicates per symbol).

Figure 2. Cytotoxicity in human cells

Six human cell types were cultured for 3 days with CRV431, CsA, or DMSO vehicle, followed by measurement of cell viability with a resazurin-based viability assay. Cytotoxicity curves for each independent experiment (grey symbols; 1-2 replicate experiments per cell line) and regression analyses of the means (black curves) are shown. The cell types included Jurkat lymphocyte cell line, HepaRG hepatocyte cell line, primary renal epithelial cells, primary dermal fibroblasts, primary bronchial smooth muscle cells, and primary umbilical vein endothelial cells.

Figure 3. CRV431 pharmacokinetics in rats

Single doses of CRV431 or CsA at 10 mg/kg were administered by oral gavage to 3 male and 3 female adult Sprague-Dawley rats. Whole blood concentrations of the two compounds were determined at the indicated time points. Data from male and female rats were combined since no statistical differences in drug exposures between genders were observed. Means and standard deviations shown.

Figure 4. Liver fibrosis in the carbon tetrachloride mouse model

Carbon tetrachloride (CCl_4) was administered intraperitoneally to male C57BL/6 mice three times per week for 6 weeks. Vehicle or compounds were administered by daily oral gavage for the entire 6 weeks: CRV431 (50 mg/kg/day), obeticholic acid (10 mg/kg/day), or a combination of CRV431 and obeticholic acid (50 and 10 mg/kg/day, respectively). (A) Liver fibrosis was assessed at the end of treatment by measuring the relative area of Sirius red staining in liver sections. P values from unpaired, parametric, 2-sided t-tests. (B) Representative staining of liver sections with Sirius Red.

Figure 5. Liver fibrosis in mouse NASH model

Vehicle or CRV431 (50 mg/kg/day) were administered orally to NASH mice in 3 independent studies. (A) Week 8-14 treatments, (B) Week 3-14 treatments, (C) Week 20-30 treatments. Liver fibrosis was assessed at the end of treatment by measuring the relative area of Sirius red staining in liver sections. P values from unpaired, parametric, 2-sided t-tests.

Figure 6. Liver tumors in mouse NASH model

Vehicle or CRV431 were administered orally to NASH mice from Week 20-30 corresponding to a late disease stage characterized by liver tumor development. Tumor burden at the end of treatment was assessed by the number of tumors (A) and a composite score based on the number and size of tumors (B; 0-7 scale). P values from unpaired, nonparametric, 2-sided t-tests. (C) Representative images of liver tumors and tumor burden scores.

TABLES

Table 1. Inhibition of multiple cyclophilins

Cyclophilin isoform	CsA IC_{50} (nM)	CRV431 IC_{50} (nM)	IC_{50} fold-difference
PPIA (Cyp A)	25.6	2.5	10.2
PPIB (Cyp B)	11.5	3.1	3.7
PPIF (Cyp D)	10.1	2.8	3.6
PPIG (Cyp G)	27.7	7.3	3.8

JPET Fast Forward. Published on August 12, 2019 as DOI: 10.1124/jpet.119.261099
This article has not been copyedited and formatted. The final version may differ from this version.

Table 2. Drug potencies in immunosuppression-related luciferase reporter assays

Lymphocyte Stimulation	NFAT-Luc CsA IC_{50} (nM)	NFAT-Luc CRV431 IC_{50} (nM)	NFAT-Luc IC_{50} fold-difference	IL2-Luc CsA IC_{50} (nM)	IL2-Luc CRV431 IC_{50} (nM)	IL2-Luc IC_{50} fold-difference
PMA + A23187	3.4	204.6	60.2	8.1	300.3	36.9
CD3 + CD28 antibodies	4.5	292.2	65.4	9.0	311.5	34.6

JPET Fast Forward. Published on August 12, 2019 as DOI: 10.1124/jpet.119.261099
This article has not been copyedited and formatted. The final version may differ from this version.

Table 3. Drug transporter inhibition

Transporter	Test system	CRV431 IC_{50} (µM)	CsA IC_{50} (µM)	CRV431 inhibitory potency vs CsA
P-gp	Caco-2	> 50	1	> 50x less
BCRP	MDCKII-BCRP	23	3	7.7x less
BSEP	Vesicles	1.42	0.42	3.4x less
MRP2	Vesicles	20.7	10	2.1x less
OATP1B1	HEK293	0.3	0.04	7.5x less
OATP1B3	HEK293	0.6	0.08	7.5x less
OAT1	HEK293	> 50	> 50	same (no inhibition)
OCT2	HEK293	> 50	> 50	same (no inhibition)
OAT3	HEK293	0.473	> 10	> 21x more
NTCP	HEK293	45.3	1	> 45x less
MATE-1	HEK293	> 100	> 100	same (no inhibition)
MATE-2	HEK293	> 100	> 100	same (no inhibition)

JPET Fast Forward. Published on August 12, 2019 as DOI: 10.1124/jpet.119.261099
This article has not been copyedited and formatted. The final version may differ from this version.

Table 4. CRV431 concentrations in blood and liver

Species	Study Treatments	mg/kg/ day	Day of Dosing	Hours Post-Dose	n	Blood µg/ml	Liver µg/g	Liver:Blood [CRV431] Ratio
Mouse	NASH	50	189	3	10	1.4 ± 1.5	11.6 ± 9.0	11.9 ± 8.5
Mouse	CCl_4	50	42	4	9	1.2 ± 0.5	14.5 ± 2.9	15.4 ± 10.4
Rat	-	30	7	12	6	1.8 ± 0.3	11.7 ± 1.9	6.6 ± 1.1
Rat	-	30	7	24	6	1.3 ± 0.2	6.0 ± 1.4	4.8 ± 1.1
Rat	-	250	7	12	6	3.2 ± 0.7	23.4 ± 3.4	7.6 ± 1.8
Rat	-	250	7	24	6	2.9 ± 0.6	15.2 ± 4.0	5.3 ± 0.6

CCl_4, carbon tetrachloride; means ± S.D.

JPET Fast Forward. Published on August 12, 2019 as DOI: 10.1124/jpet.119.261099
This article has not been copyedited and formatted. The final version may differ from this version.

Table 5. NASH mouse model data

	Week 3-14 Treatment		**Week 8-14 Treatment**		**Week 20-30 treatment**	
	Vehicle	CRV431	Vehicle	CRV431	Vehicle	CRV431
Body weight	39.7 ± 6.0	33.5 ± 5.2 (P < 0.05)	30.0 ± 7.1	26.1 ± 5.1	48.9 ± 8.3	41.6 ± 8.9
Liver weight	1.60 ± 0.44	1.28 ± 0.28	1.28 ± 0.19	1.35 ± 0.28	4.17 ± 0.74	3.04 ± 1.19 (P < 0.05)
Blood glucose	333 ± 70	319 ± 79	467 ± 123	463 ± 143	442 ± 90	405 ± 134
Steatosis score	2.0 ± 1.1	1.3 ± 1.1	1.5 ± 0.9	2.0 ± 0.5	n/a	n/a
Inflammation score	2.3 ± 0.8	1.5 ± 0.7	1.8 ± 1.5	2.4 ± 0.7	n/a	n/a
Ballooning score	1.4 ± 0.5	0.9 ± 0.6	1.5 ± 0.8	1.8 ± 0.5	n/a	n/a
NAS score	5.7 ± 1.6	3.7 ± 2.2 (P < 0.05)	5.4 ± 2.4	6.1 ± 1.1	n/a	n/a
Sirius Red %	3.10 ± 1.03	1.96 ± 0.72 (P < 0.05)	1.90 ± 0.79	1.02 ± 0.48 (P < 0.05)	2.88 ± 1.20	1.62 ± 0.57 (P < 0.05)
Tumor number	n/a	n/a	n/a	n/a	8.1 ± 2.8	4.5 ± 4.4
Tumor score	n/a	n/a	n/a	n/a	4.7 ± 1.9	2.25 ± 2.0 (P < 0.05)

Mean ± S.D.; P values from unpaired, 2-sided t-tests between vehicle and CRV431 treatment groups. Nonparametric t-tests for scores and parametric t-tests for all other variables. N values shown in Figure 5.

JPET Fast Forward. Published on August 12, 2019 as DOI: 10.1124/jpet.119.261099
This article has not been copyedited and formatted. The final version may differ from this version.

FIGURES

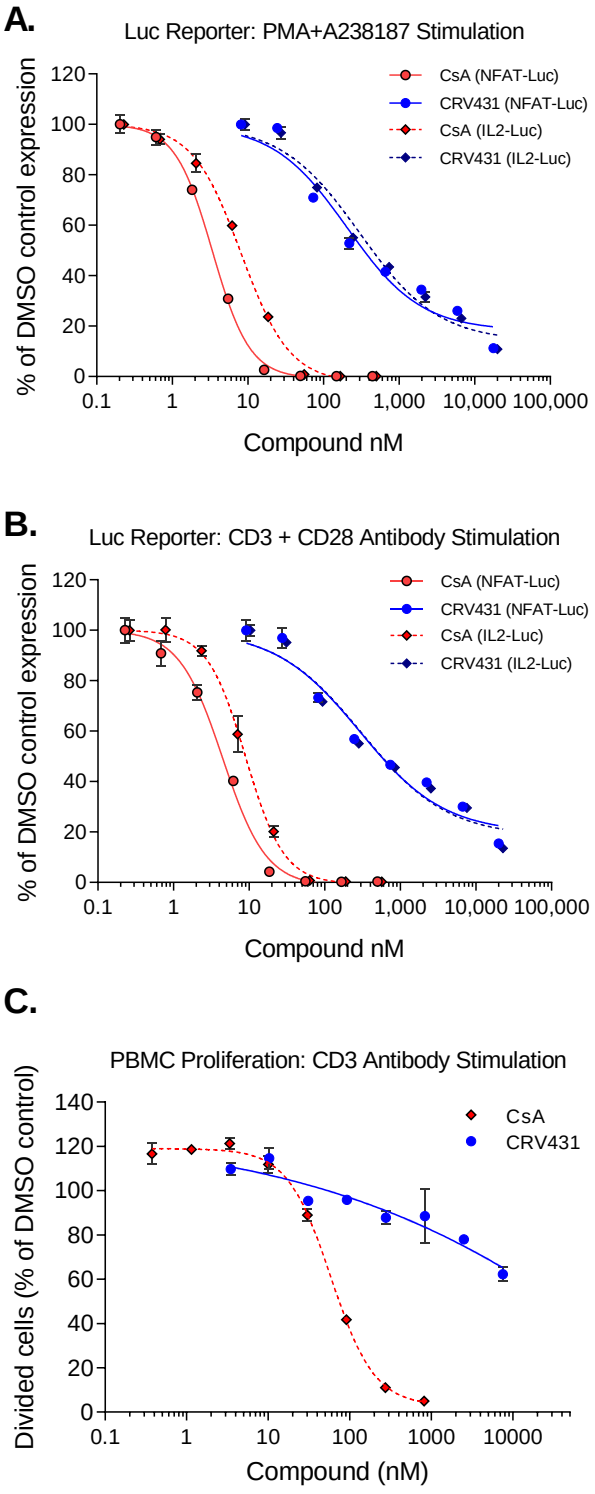

Figure 1

JPET Fast Forward. Published on August 12, 2019 as DOI: 10.1124/jpet.119.261099
This article has not been copyedited and formatted. The final version may differ from this version.

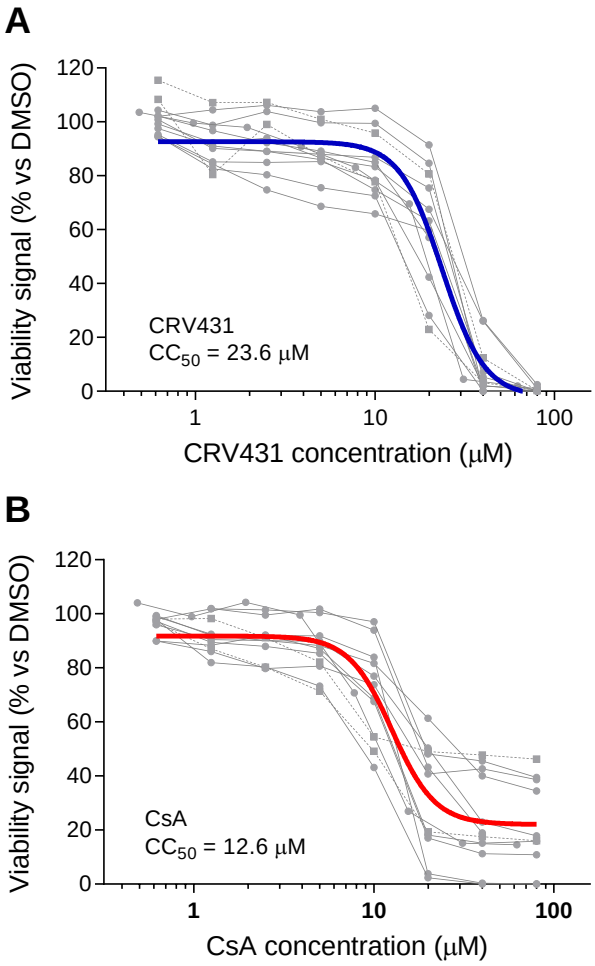

Figure 2

JPET Fast Forward. Published on August 12, 2019 as DOI: 10.1124/jpet.119.261099
This article has not been copyedited and formatted. The final version may differ from this version.

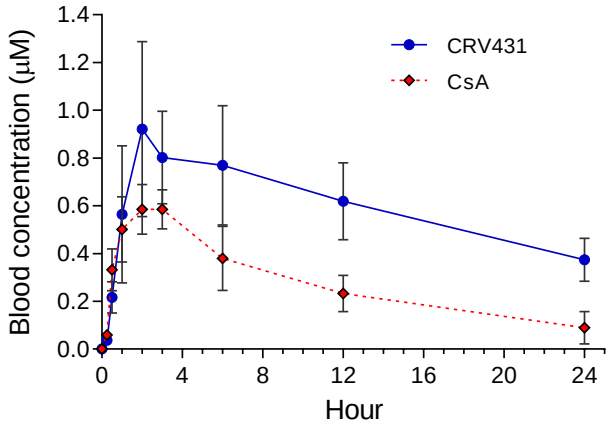

Figure 3

JPET Fast Forward. Published on August 12, 2019 as DOI: 10.1124/jpet.119.261099
This article has not been copyedited and formatted. The final version may differ from this version.

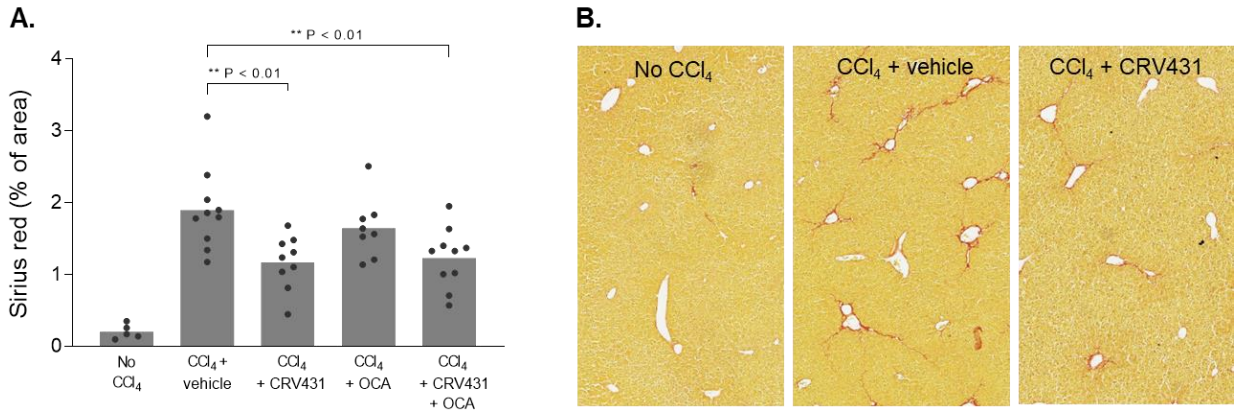

Figure 4

JPET Fast Forward. Published on August 12, 2019 as DOI: 10.1124/jpet.119.261099
This article has not been copyedited and formatted. The final version may differ from this version.

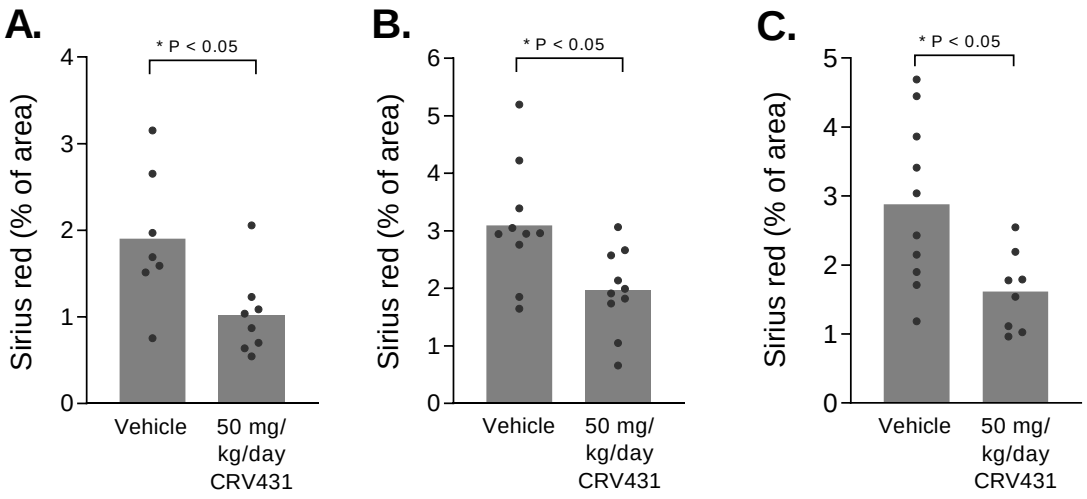

Figure 5

JPET Fast Forward. Published on August 12, 2019 as DOI: 10.1124/jpet.119.261099
This article has not been copyedited and formatted. The final version may differ from this version.

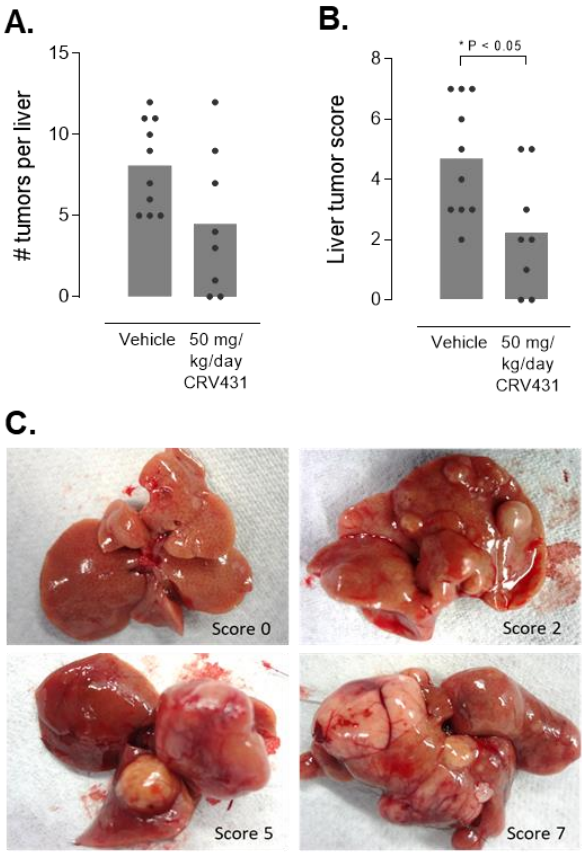

Figure 6